International Journal of Lightweight Materials and Manufacture 4 (2021) 468–479

Contents lists available at ScienceDirect

International Journal of Lightweight Materials and Manufacture

journal homepage: https://www.sciencedirect.com/journal/international-journal-of-lightweight-materials-and-manufacture

Original Article

Carbon-fiber reinforced polymer composites: A comparison of manufacturing methods on mechanical properties

Andrew Y. Chen, Sebastian Baehr, Austin Turner, Zilan Zhang, Grace X. Gu*

Department of Mechanical Engineering, University of California, Berkeley, CA 94720 USA

ARTICLE INFO

Article history:
Received 25 December 2020
Received in revised form
1 March 2021
Accepted 4 April 2021
Available online 14 April 2021

Keywords:
Fiber-reinforced composites
3D-printing
Additive manufacturing
Mechanical properties
Hand layup
Laminated beam theory

ABSTRACT

Carbon-fiber reinforced polymer composite materials are used throughout industry for their excellent mechanical properties; in particular, these composites boast high specific stiffnesses and specific strengths. However, current limitations on manufacturing, which vary greatly based on the technology that is utilized, restrict access to composite materials in a variety of applications. Traditional wet hand-layups offer a large diversity of viable constituent materials, but the fabrication geometry is limited and the manual process is time-consuming. In contrast, fiber 3D-printing (F3DP) allows for the production of complex geometries and requires little manual labor. In this study, laminates with continuous carbon fiber reinforcement printed using a commercially-available 3D printer are compared to carbon fiber fabric-resin composites produced using manual layup techniques. Cross-ply $[0,90,0,90,0]_T$ laminates were fabricated and subject to mechanical testing in uniaxial tension and flexure. After normalization with respect to fiber volume fraction, we found that the tensile strength and stiffness of cross-ply carbon fiber composites manufactured using F3DP were higher than the tensile strength and stiffness of cross-ply specimens manufactured by a traditional hand-layup method; however, the hand-layup specimens exhibited higher strength and stiffness in flexure. The difference in material properties evident between the two fabrication methods suggests that each has its own suitable application. We anticipate that further studying the failure response of printed, fiber-reinforced composite materials to various loading modalities will give insight into potential areas of improvement for F3DP material selection and printing processes, particularly relating to void reduction. On a broader scale, comparing and analyzing the mechanical properties of composite laminates produced in these various methods will provide perspective on the viability of novel additive manufacturing methods for large-scale production and industrial applications.

1. Introduction and background

Composites are commonly seen in many structural applications due to their favorable properties (e.g., high specific strength and stiffness) and the ability to overcome the intrinsic tradeoffs seen in traditional materials [1–5]. In many applications, sheets of fiber are arranged in layers and bonded together within a matrix material, forming a laminated composite structure [6,7]. In recent years, new technologies for the additive manufacturing of composites have emerged [8–11]. Specifically, for continuous carbon fiber-based composites, so-called fiber 3D printing (F3DP) allows for faster production times, more accurate parts, and more complex geometries [12].

Fiber 3D printing is primarily based on existing fused filament fabrication (FFF) processes. In general, the FFF process involves the heating and subsequent softening of thermoplastic filament followed by controlled extrusion onto the printing surface or the previous layer in a raster pattern. The thermoplastic cools after contact, solidifying and bonding with the existing material. This process is repeated in a layer-by-layer process until the part is complete. Currently, the most common method for the fabrication of composites via FFF is to use carbon-fiber or fiberglass-reinforced thermoplastics. Chopped fibers can be blended or otherwise added to commonly-used printable polymers such as acrylonitrile butadiene styrene (ABS) [13] or polyamide (PA) [14]. Stronger fiber-

* Corresponding author.
E-mail address: ggu@berkeley.edu (G.X. Gu).
Peer review under responsibility of Editorial Board of International Journal of Lightweight Materials and Manufacture.

https://doi.org/10.1016/j.ijlmm.2021.04.001

reinforced parts can also be printed via FFF by simultaneously supplying continuous fibers and traditional thermoplastic filament to the printer, allowing the fiber to impregnate the filament as it melts upon contact with a heated nozzle [15] or by capturing fiber layers between thermoplastic layers [16].

Empirical testing demonstrated in the literature has confirmed the result predicted by models such as the rule of mixtures: namely, that the method of adding fibers to a thermoplastic material generally results in an increase in elastic modulus and material strength at the expense of a reduced ductility. Ning et al. [17] found that increasing the amount of carbon fiber in ABS first increased, then decreased both elastic modulus and tensile strength above a certain weight fraction (10 wt%). The subsequent decrease in strength and modulus of elasticity is explained by a sudden increase in the porosity of the material, which itself is a major limitation of the FFF printing process. Porosity, along with void spaces caused by poor adhesion between layers, was commonly reported as a principal cause of failure-inducing defects in printed laminates [18,19]. Naranjo-Lozada et al. [20] found, however, that a chopped-fiber reinforced nylon material showed an increase in elastic modulus of up to 2.97 times that of pure printed nylon, whereas continuous fiber-reinforced prints demonstrated a 25-fold increase in elastic modulus.

In addition to the modification of existing printer hardware to accommodate chopped or continuous fibers within the thermoplastic filament, there are commercially available printers, such as the Markforged X7 [21], which are designed from the ground up for the purpose of printing continuous fiber composite parts. The X7 uses proprietary materials in a closed ecosystem; dual extrusion is used to supply continuous fiber reinforcement alongside a thermoplastic matrix material. The arrangement and orientation of layers may be customized in the pre-print slicer software; however, the printer is capable of printing continuous fiber only on the inside of printed parts, and the continuous fiber material contains additives that facilitate the FFF printing process, resulting in a reduction in longitudinal and flexural strengths compared to raw carbon fibers [12]. Despite this, Blok et al. [22] found an order of magnitude increase in the normalized tensile modulus and tensile strength of Markforged-printed continuous fibers compared to printed short fibers. The porosity of the continuous fiber material was an eightfold increase over that of the short fiber configuration.

In addition to material selection, print process parameters such as filament extrusion speed and orientation, printing temperature, and infill density are also important factors to control in FFF printing. With respect to printable composite materials, the effect of varying process parameters on material properties has been evaluated in the literature for a number of printing configurations. Specifically, as with hand-layup composites, there is a strong dependence of laminate material properties on fiber orientation [23], for both short, chopped fibers [24] and continuous fibers [25,26]. Laminate strength and stiffness are maximized when the fiber orientation is parallel to the direction of loading; however, the degree of anisotropy is also amplified when fibers are all oriented in one particular direction [27].

In many applications, the composite part is subject to a compound, multiaxial loading, and it becomes necessary for the part to withstand stresses in multiple directions. To address this, a common laminate construction method called the cross-ply structure alternates layers of fibers in a $[0,90,0, \ldots ,90,0]_T$ orientation. Cross-ply laminates are widely used in applications where the loading state of the composite is bidirectional; this is especially common in the aerospace industry. These laminates are assumed to be "specially orthotropic": any applied load creates strain effects only in directions along the load or orthogonal to it. Nonlinear shear coupling effects are not present, allowing for simpler theoretical models based on linear transformations to be used for analysis.

Wet hand layups, which may include the use of vacuum bagging or compression molding, and the use of "pre-preg" fabric [28] are the most prevalent "traditional" composite manufacturing processes for cross-ply laminates. In general, these methods allow large, often woven, sheets of composite material to be layered above a mold or mandrel, saturated with thermosetting epoxy resin (with the exception of pre-preg fabric, which is infused with resin during its manufacturing), and allowed to cure. Many types of materials can be used in a hand layup-based process; common fibrous materials include carbon fibers, glass fibers, and jute fibers. Of these fibers, carbon exhibits the highest strength and stiffness. The surface finish and dimensional consistency of the finished product, as well as the reduction of void space, can be improved by using elevated temperatures and elevated pressures. For this reason, vacuums, ovens, and autoclaves are often used to cure parts [29]. However, many matrix materials such as epoxy resins can be cured at ambient environmental conditions, allowing for flexibility in the fabrication process.

Although it is known that in general, layer orientation affects the material properties of a laminated composite part due to changes in the mesostructure [30], the difference between printed and traditionally-manufactured cross-ply laminates is not well understood. In this paper, we aim to directly compare the material properties of cross-ply laminates produced by F3DP and by a hand layup method, normalizing results to a common fiber volume fraction to account for the variation in the matrix phase present between the constituent materials. The laminate produced and studied using each method is a representative sample of the product that is produced by the corresponding method, providing a direct comparison of manufacturing methods without significant process parameter modification. A carbon fiber and epoxy resin composite will be used to represent the traditionally manufactured material, while a directly-printable nylon and carbon fiber composite will be used to represent the F3DP-produced material. While the constituent materials produced by the two processes differ, the normalization process enables a direct comparison between laminates. Two loading modalities, which represent the most common use cases of composite parts, are studied: uniaxial tension and flexure. Theoretical models and a computed finite-element simulation are used to provide a point of comparison for the mechanical tests and to evaluate the reliability of assumptions used in the approximation of composite laminate properties. Because the cross-ply structure is important to many structural applications in engineering, the objective of this work is to help inform manufacturers and designers about the relative viability of novel additive manufacturing methods for carbon-fiber composites compared to more labor-intensive traditional processes with respect to material properties. While installation and material costs, production time, and other factors are also important points of consideration especially at larger scales, the present work aims to establish a fair basis of comparison from a structural, material point of view.

2. Theory and calculation

2.1. Theoretical models for specially orthotropic cross-ply laminates

Models for material properties developed from first principles of continuum mechanics were used to evaluate the theoretical stiffness of each material under an axial, tensile load and under a flexural load. First, a rule-of-mixtures approach as described by

Gibson [31] was used to predict the elastic modulus of the material in the longitudinal direction (parallel to the principal, 0° fiber orientation). A second approach using the laminated beam theory developed from the Bernoulli-Euler theory of beams was used to calculate the same laminate elastic modulus independently. The laminated beam theory assumes a perfect bonding condition such that any bending moment imparted on the composite laminate results in plane sections normal to the central axis remaining orthogonal during deformation [31,32]. Finally, the computed material properties of each laminate were normalized to a fiber volume fraction $V_f = 0.35$ which well approximates the fiber content in most composite material applications.

In the analysis, a state of "plane stress" is assumed; that is, there is assumed to be no loading across the thickness-dimension of the material. In plane stress, cross-ply laminates experience no shear coupling effects across layers and are hence considered specially orthotropic materials [33]. For the laminate as a whole, properties in orthogonal directions are not assumed to be equal.

The analysis begins with a single-ply laminate (i.e. a lamina), with a defined unit vector in the direction parallel to the principal (0°) fiber orientation ("1-direction") and a second unit vector orthogonal to the first ("2-direction"). Because of the ability of the fibers to carry load primarily in their longitudinal direction, the material properties of the lamina differ between the 1- and 2- directions. Notably, the elastic modulus $E_i$of the material in a specified direction i is nonconstant, $E_1 \neq E_2$. The shear modulus G_i of the material is also nonconstant, $G_1 \neq G_2$.

Furthermore, when a load is applied to the lamina, it deforms in both the loading direction i and the perpendicular direction j; Poisson's ratio ν_{ij} describes the ratio of strain in the j-direction to the strain in the i-direction, $\nu_{ij} = -\varepsilon_j/\varepsilon_i$. For the lamina directions 1 and 2, the Poisson's ratios are related by the equation

$$\nu_{12} = \frac{E_1}{E_2}\nu_{21} \tag{1}$$

Therefore, the total strain ε_i in a particular direction (i) as a result of an applied stress can be expressed as

$$\varepsilon_i = \frac{\sigma_i}{E_i} - \frac{\nu_{ij}\sigma_j}{E_i} = \frac{\sigma_i}{E_i} - \frac{\nu_{ji}\sigma_j}{E_j} = \frac{\sigma_i}{E_i} - \nu_{ji}\varepsilon_j \tag{2}$$

where the first term describes the stiffness-based response to the direct applied stress, and the second term is due to contraction effects stemming from strains in the orthogonal direction [34].

2.1.1. Rule of mixtures

The rule of mixtures equation develops the laminate modulus in the 1-direction as a volume-fraction weighted average of the elastic modulus of each lamina (ply):

$$(E_{laminate})_1 = E_1V_1 + E_2V_2 \tag{3}$$

Here, V_1 is the volume fraction of longitudinal plies, and V_2 is the volume fraction of transverse plies. E_1 corresponds to the elastic modulus of a single lamina loaded in the longitudinal direction, whereas E_2 corresponds to the elastic modulus of a single lamina loaded in the transverse direction.

In each direction, the elastic modulus of the lamina is itself computed by a rule-of-mixtures formula which depends on the volume fraction of fiber $V_f$in that lamina,

$$E_1 = E_fV_f + E_m\left(1 - V_f\right) \tag{4}$$

$$E_2 = \left(\frac{V_f}{E_f} + \frac{1 - V_f}{E_m}\right)^{-1} \tag{5}$$

Here, $E_f$represents the fiber stiffness, and E_m represents the matrix material stiffness. In general, the matrix material is taken to be isotropic.

2.1.2. Laminated beam theory

For the orthotropic, plane stress condition, the material properties of the lamina can be summarized in a 3-by-3 matrix, called the reduced stiffness matrix $[Q]$. The reduced stiffness matrix relates resultant longitudinal, transverse, and shear strains to applied longitudinal, transverse, and shear stresses:

$$\begin{pmatrix}\sigma_1\\ \sigma_2\\ \tau_{12}\end{pmatrix} = \begin{pmatrix}Q_{11} & Q_{12} & 0\\ Q_{12} & Q_{22} & 0\\ 0 & 0 & Q_{66}\end{pmatrix}\begin{pmatrix}\varepsilon_1\\ \varepsilon_2\\ \gamma_{12}\end{pmatrix} = [Q]\begin{pmatrix}\varepsilon_1\\ \varepsilon_2\\ \gamma_{12}\end{pmatrix} \tag{6}$$

In particular, for the laminae oriented at 0°, the nonzero entries are given by $Q_{11} = \frac{E_1}{1-\nu_{12}\nu_{21}}$, $Q_{22} = \frac{E_2}{1-\nu_{12}\nu_{21}}$, $Q_{12} = \frac{\nu_{12}E_2}{1-\nu_{12}\nu_{21}}$, and $Q_{66} = G_{12}$. The reduced stiffness matrix of the laminae oriented at 90°, $[\overline{Q}]$, can be calculated using the transformation relation $[\overline{Q}] = [T]^{-1}[Q][T]^{-T}$, where entries of the matrix $[T]$ are trigonometric functions of the angle θ between the plies represented by $[Q]$and $[\overline{Q}]$:

$$[T] = \begin{pmatrix}\cos^2(\theta) & \sin^2(\theta) & 2\sin(\theta)\cos(\theta)\\ \sin^2(\theta) & \cos^2(\theta) & -2\sin(\theta)\cos(\theta)\\ -\sin(\theta)\cos(\theta) & \sin(\theta)\cos(\theta) & \cos^2(\theta) - \sin^2(\theta)\end{pmatrix} \tag{7}$$

Here, $[T]^{-T}$indicates the transpose of the inverse of the matrix $[T]$. Because the angle between the plies is exactly 90°, the trigonometric terms simplify greatly and the matrix $[\overline{Q}]$has nonzero entries $\overline{Q}_{22} = Q_{11}$, $\overline{Q}_{11} = Q_{22}$,$\overline{Q}_{12} = Q_{12}$, $\overline{Q}_{66} = Q_{66}$.

For a laminate made of five plies, with the $[0,90,0,90,0]_T$ ply configuration, the extensional stiffness matrix $[A]$, which provides the laminate-level relation between normal stresses and strains, is related to the thickness t of each lamina and the reduced stiffness matrix $[Q]_k$ for each ply using

$$A_{ij} = \sum_{k=1}^{n}\left[Q_{ij}\right]_k t_k \tag{8}$$

In a plane stress loading condition, the components of the extensional stiffness matrix $[A]$ are used to derive the overall longitudinal stiffness of the n-ply laminate by considering Poisson effects [21]. For a specially orthotropic material, all the fibers are oriented either along the loading direction or orthogonal to it, meaning that $A_{16} = A_{61} = 0$ and the laminate stiffness can be written as

$$(E_{laminate})_1 = \frac{1}{nt}\left(A_{11} - \frac{A_{12}^2}{A_{22}}\right) \tag{9}$$

Here, the nt term accounts for the overall thickness of the n-ply laminate with uniform plies of thickness t. The analysis is more complex for nonsymmetric laminates or laminates that contain plies not limited to 0° or 90°; in these *angle-ply laminates*, shear coupling effects must be taken into consideration.

The flexural modulus of a laminated beam having n plies of uniform thickness derived using the theory of laminated plates [31,35] is given by

$$(E_{laminate})_f = \frac{8}{n^3}\sum_{j=1}^{\frac{n}{2}}(E_1)_j\left(3j^2 - 3j + 1\right) \tag{10}$$

Here, $(E_1)_j$ is the elastic modulus of the jth ply in the 1-direction. This expression, valid for an even number of plies in a cross-ply arrangement, also assumes the same geometric constraints: that (i) the plies are perfectly bonded, (ii) the loading is uniaxial in tension, and (iii) geometric constraints hold for the laminate about the neutral axis during any type of flexure. This theory was developed extensively by Pagano [36]. The five-layer laminate used in this study has an odd number of plies, but it suffices to equivalently use $n' = 2n = 10$ plies of thickness $t' = t/2$ in the calculation, which alternates also in a $[(0,90)_2]_5$ pattern such that the flexural modulus equation is satisfied and successive plies are oriented at right angles to the last.

2.1.3. Normalization

Material properties of the hand-layup materials were obtained from the manufacturer specifications. The constituent material properties for the printed parts were adapted from Ghebretinsae [37] and the testing data provided by Markforged [38]. A study by van der Klift et al. [39] found that the commercial filament used as "continuous fiber reinforcement" in the Markforged printer itself contains a fiber volume fraction of $V_f = 0.345$, with the remaining 65.5% by volume consisting of polymer adhesives and other constituents with negligible stiffness. As such, the stiffness of the continuous fibers used to model the Markforged fiber material was taken to be 34.5% that of standard carbon fiber yarn [37]. The proprietary Onyx material, which consists of nylon and chopped carbon fiber, was characterized by Damodaram [40] and is used as the matrix material in the printed composite. The volume fraction of fiber and the volume fraction of Onyx matrix material in the printed parts were taken from the Markforged slicer; for the layer scheme chosen, the fiber volume fraction is 20.9%.

However, because the materials have different fiber volume fractions, it is necessary to normalize the fiber content before comparing calculated properties. The normalization procedure is adapted from Blok et al. [22]. For a laminate with a fiber volume fraction V_f' and measured elastic modulus E', the elastic modulus is adjusted using the formula

$$E_{normalized} = \frac{V_f}{V_f'}E' \tag{11}$$

Here, all measured quantities are normalized by fiber volume fraction to a common value of 35%, $V_f = 0.35$.

Table 1
Calculated lamina material properties. Material properties (elastic modulus along and normal to the fiber orientation, Poisson's ratio, and shear modulus) for each lamina, or ply, were computed using raw material data and the fiber volume fraction V_f.

	Hand layup	Printed parts
V_f	0.31	0.209
E_1 [GPa]	71.24	13.64
E_2 [GPa]	1.49	1.76
ν_{12}	0.297	0.247
G_{12} [GPa]	27.46	0.73

Table 2
Calculated laminate material properties for $[0,90,0,90,0]_T$ stacking sequence.

	Hand layup		Printed parts	
	Raw	Normalized	Raw	Normalized
E_1, rule of mixtures [GPa]	43.34	48.93	8.892	14.89
E_1, laminated plate theory [GPa]	43.42	49.02	8.952	14.99
E_f, laminated plate theory [GPa]	46.69	52.27	9.462	15.84

Using the theory developed above, and the data from Refs. [37–40], the lamina and laminate properties in Tables 1 and 2 were calculated.

3. Materials and methods

3.1. Sample fabrication

In order to directly compare the methods of wet hand layup and F3DP, sets of identical samples were fabricated using each process (Fig. 1a). Two types of samples were fabricated: tensile "dog-bones" and flexure strips, following the geometry specified by the ASTM testing standards [41,42]. Fig. 1c shows the sample geometry for all tests used in the study; the minimum length dimension of the hand-layup flexure sample, which is dependent on the laminate thickness, was determined after curing when a precise thickness measurement was taken.

3.1.1. Hand layup

A wet layup was completed by hand using sheets of unidirectional carbon fiber [Hexcel, Stamford, Connecticut, USA], and a two-part epoxy resin [TAP Plastics, El Cerrito, California, USA] was used as the matrix material. Using the manufacturer's specification for density, the equivalent of 31 vol% resin to fiber weight was measured and prepared according to the manufacturer's instructions. A flat, clean work surface was prepared and a sheet of stretched polyethylene terephthalate (PET) film was placed on the work surface to facilitate the removal of the part after curing. One by one, the sheets of carbon fiber were laid atop the PET film and wetted evenly with epoxy resin. A paintbrush was used to ensure thorough and uniform saturation. Each sheet was placed on top of the last in alternating directions to create a five-layer, $[0,90,0,90,0]_T$ laminate. After the final fiber layer was wetted, another sheet of PET film was placed on the assembled laminate. The laminate was weighed down and was allowed to cure at room temperature for a period of 24 h. After the laminate cured fully, it was cut into the appropriate testing geometry using a water-jet cutter. In total, two sheets were made, and the location within each sheet of the testing specimens were chosen using an even distribution; in this way, the test specimens formed a representative sample of each fabricated sheet.

3.1.2. Printed parts

The printed parts were manufactured using the Markforged X7 printer, which uses continuous extrusion to produce fiber-reinforced composites on a layer-by-layer basis. After STL files were generated of each specimen geometry, the printing settings were adjusted in the slicer so that the printed parts mimicked the $[0,90,0,90,0]_T$ structure of the wet layup parts as closely as possible (Fig. 1b). The carbon-fiber based "continuous fiber reinforcement" was inlaid in the Onyx matrix material such that there was symmetry above and below the midplane of the printed part; the center of the middle set of fiber layers coincided with the midplane of the part. The continuous fiber layers were placed two at a time, with each set alternating by 90° relative to the last. Therefore, the final

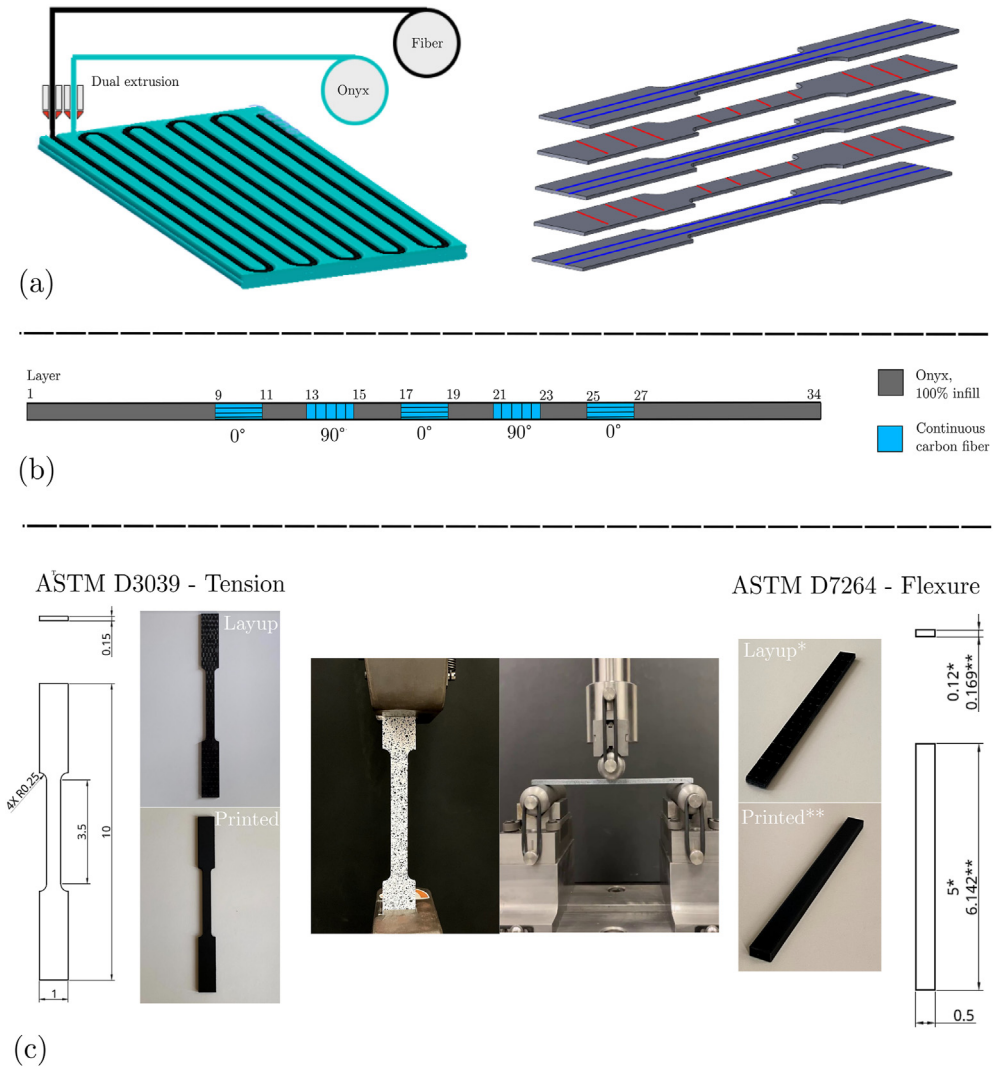

Fig. 1. (a) Two fabrication methods for continuous-fiber reinforced composites. In dual-extrusion F3DP, two nozzles extrude continuous fiber filament alongside a thermoplastic matrix material in a raster pattern determined in the pre-print slicer. In the hand-layup process, sheets of continuous fiber are arranged in a cross-ply pattern and bonded together with a thermosetting material. (b) The layer configuration used in the printed parts to mimic the $[0,90,0,90,0]_T$ cross-ply structure. (c) Specimen dimensions and test setup used to obtain tensile (left) and flexural (right) mechanical properties of the hand-layup and printed parts.

part contained two layers per fiber orientation with two layers of pure Onyx material separating consecutive fiber layers. There were ten total layers of continuous fiber reinforcement. Above and below the topmost and bottommost fiber layers, pure Onyx was used to fill out the specimen height so that the geometry specified by each ASTM standard was realized.

3.2. Sample testing

3.2.1. Tensile testing

Tensile testing was conducted following ASTM standard D3039 [41]. The dog-bone samples were placed in an Instron 5980 Series Universal Testing System and extended in uniaxial, monotonic tension at a strain rate of 2 mm/min until failure. Fourteen hand-layup specimens were fabricated, and seven specimens were printed. During testing, specimen #9 in the hand-layup cohort experienced abnormalities, and consequently the data for that test was dismissed.

The Instron Universal Testing System reports displacement δ and load P, taken at intervals in time. To normalize these values to engineering stress σ and engineering strain ε, the following equations are used:

$$\sigma = \frac{P}{A_c} \tag{12}$$

$$\varepsilon = \frac{\delta}{L_0} \tag{13}$$

The cross-sectional area A_c of each sample and the original gauge length L_0 of each sample were measured prior to testing.

3.2.2. Flexural testing

Flexure testing was conducted using a procedure adapted from ASTM standard D7264 [42]. The samples were rectangular in geometry. A three-point bend setup with a 32:1 span-to-thickness was used for each sample set. The contact points had a nose radius of 0.5 in (12.7 mm), which increased compliance in the flexure samples. To compensate for this effect, the displacement rate was increased from the ASTM standard setting (1 mm/min) to a speed of 2 mm/min until failure. Four hand-layup specimens and

four printed specimens were tested. The tested samples were chosen at random from the set of fourteen hand-layup specimens and seven printed specimens that were manufactured. The Instron 5980 Series testing system reports displacement δ at the mid-span of the sample and load P, taken at intervals in time. To normalize these values to flexural stress σ_f and flexural strain ε_f, the following equations are used [42]:

$$\sigma_f = \frac{3PL_{span}}{2bh^2} \tag{14}$$

$$\varepsilon_f = \frac{6\delta h}{L_{span}^2} \tag{15}$$

The span distance L_{span} is set at exactly 32 times the thickness h of each sample; the sample thickness and width b were measured prior to testing. During testing, specimen #4 in the hand-layup cohort experienced abnormalities, and consequently the data for that test was dismissed.

3.2.3. Digital image correlation

Before testing, a subset of the specimens was spray-coated with white paint and randomly positioned black specks. The samples were recorded from the front side. From the recordings, a sequence of static images are taken at regular intervals, and the DICe engine [43] is used to track positions of individually-selected points along the sample. Digital image correlation (DIC) allows for a secondary method of calculating and visualizing displacements (and therefore strains), and is used to corroborate the data obtained from the mechanical testing measurements.

4. Results and discussion

4.1. Tensile testing

After the specimens were tested as described in Section 3.2, the raw data was converted to stress-strain data, plotted, and analyzed to obtain relevant material properties. In tensile testing, the hand-layup samples had an average ultimate tensile strength of 164.57 MPa, with a standard deviation of 32.3 MPa; the printed parts had an average ultimate tensile strength of 126.88 MPa with a standard deviation of 9.5 MPa. The average first-ply failure strains (and standard deviations) were 0.6378% (0.1357%) and 0.9625% (0.2073%) for the hand-layup and printed samples, respectively. The average ultimate failure strains (and standard deviations) were 3.7829% (0.4419%) and 3.9748% (0.3537%). In both the hand-layup and printed cohorts, the maximum load, corresponding to the ultimate tensile strength, was borne by the specimen just before failure. A coefficient of variation is calculated for each sample set to gauge the repeatability of each manufacturing method. A piecewise linear fit (with $n = 2$ segments) was performed on the data sets to obtain the modulus of elasticity before and after first-ply failure. The results are summarized in Table 3. Fig. 2a–b shows representative tensile stress-strain curves from the hand layup and printed cohorts, respectively.

In addition to the data returned by the Instron testing machine, digital image correlation (DIC) was used to estimate the strain-to-failure of four tensile specimens (Fig. 3a). Maximum strain values, corresponding to the instant before failure, were computed using five separate points on each tension specimen. In general, DIC showed consistent results but in each case underestimated the experimental results for strain, likely due to poor point tracking at the top of the specimen (the location of greatest displacement) because of the presence of shadows. For reported measurements of material properties, the Instron testing machine data was used.

In tension, failure of the specimens occurred in the gauge section, near the beginning of the radius at the top end of the sample. A similar failure mechanism has been observed by Dickson et al. [26]; failure in the neck of the dog-bone shape was attributed to shear forces localized to this region by the fiber alignment. A strain-controlled computed simulation with a displacement rate of 10 mm/min (Fig. 3b) reveals this pattern of stress concentration around the neck of the specimen; the location of greatest stress experiences a stress concentration factor of up to 1.33.

Failure occurred laterally across the sample width, and every sample failed in the characteristic brittle failure mode of composite laminates. In the stress-strain graphs of both cohorts, a piecewise-linear behavior was observed up to ultimate specimen failure. The neck in the stress-strain plot is taken to be the onset of “first-ply failure”; the stiffness of the composite decreases after this point and is roughly constant until ultimate failure. In particular, first-ply failure of the tested specimens likely corresponds with failure of fibers within a lamina oriented at 90° to the direction of tension. Due to the alternating orientation scheme of each lamina relative to the last, and the presence of matrix material between fiber layers, the neighboring 0° plies sandwich the failed ply and prevent failure propagation. Hence, the composite continues to function structurally, albeit with lower stiffness. However, as the load on the composite is increased, fibers in successive plies fail until the laminate can no longer sustain the load, at which point the specimen fails catastrophically. These later ply failures happen in quick succession near the failure strain of the composite.

This delamination pattern was evident in the collected data. In a subset of the samples, the distinct occurrence of successive-ply failures was evident, as noted by multiple unique drop-off points in the stress-strain curves occurring near ultimate failure (Fig. 2e). This demonstrates concretely that the specimens failed on a layer by layer basis until the eventual catastrophic failure of the laminate. This behavior is clearly evident in the testing data produced by four of the seven printed parts and five of the thirteen hand-layup parts. When this behavior was observed, the second segment of the piecewise linear fit was adjusted to fit only the portion of the stress-strain curve associated with the second linear regime.

Inspection of the failure location on each sample further reveals the mechanism by which each sample type failed. During failure, delamination occurred at the broken portion of the specimen; exposed fibers (fiber pull-out) are also evident in both the printed

Table 3
Empirically-determined material properties - tensile testing.

Average values, no V_f normalization	Hand layup, n = 13			Printed, n = 7		
	Mean	St. Dev.	CV	Mean	St. Dev.	CV
Ultimate tensile strength [MPa]	164.57	32.27	0.196	126.88	9.48	0.074
Elastic modulus [MPa]	6628.08	1042.47	0.157	4757.62	151.68	0.031
Elastic modulus after first-ply failure [MPa]	3779.99	666.98	0.176	2693.58	238.98	0.088
First-ply failure strain	0.006378	0.001357	0.212	0.009625	0.002073	0.215
Laminate failure strain	0.037829	0.004419	0.116	0.039748	0.003537	0.088

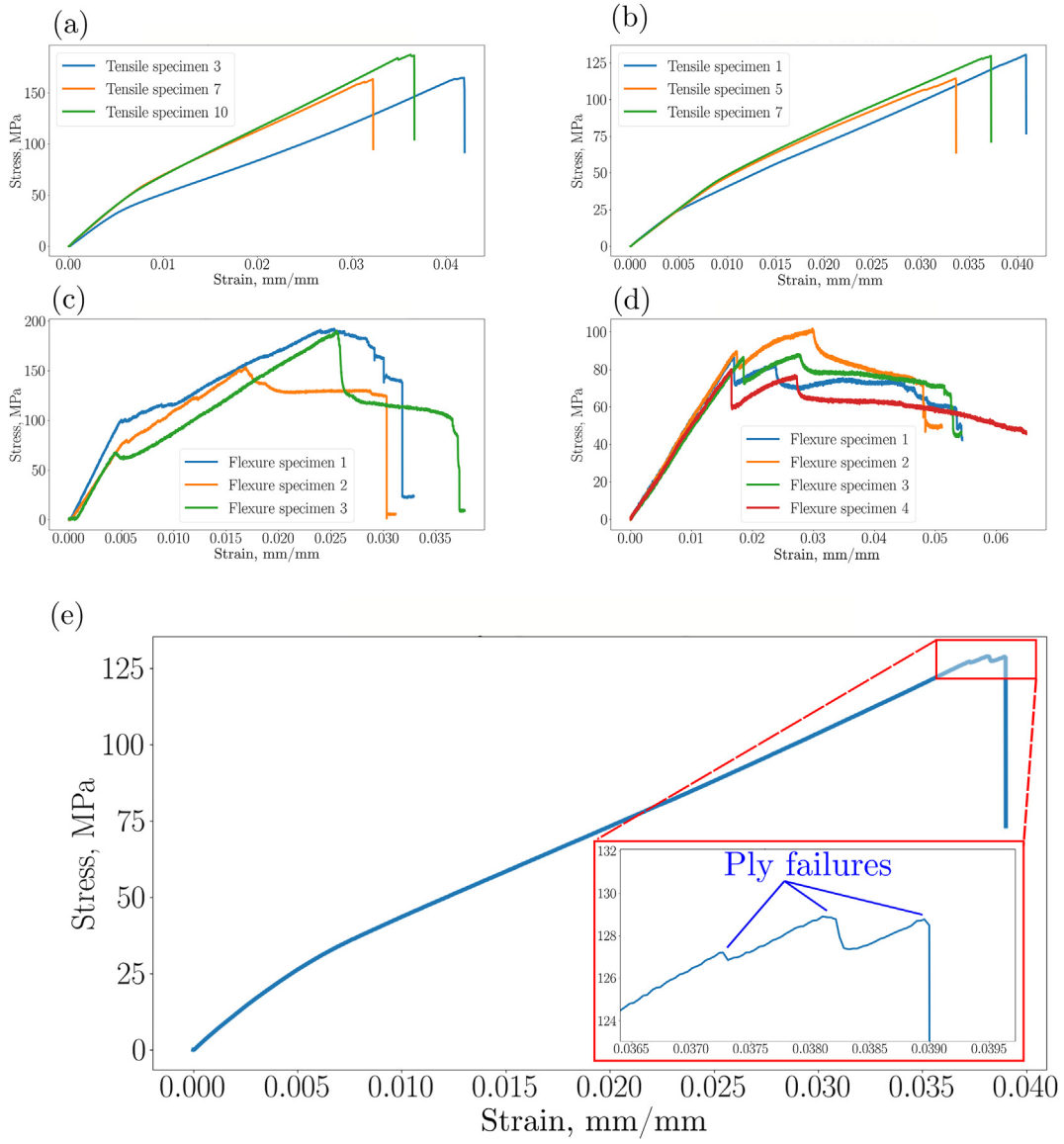

Fig. 2. Representative stress-strain curves obtained from testing. (a) Hand-layup tension specimens. (b) Printed tensile specimens. (c) Hand-layup flexure specimens. (d) Printed flexure specimens. (e) Tensile stress-strain curve of a hand-layup specimen that experienced distinct ply failures near ultimate failure (inset).

and hand-layup parts (Fig. 3c). The printed parts also experienced separation between the outer Onyx layers and the inner continuous-fiber layers (Fig. 3d), with the Onyx material chipping away near the site of initial crack propagation. This suggests that the bonding between the Onyx and continuous fiber materials is comparatively weaker than the bonding of either material to itself. However, the failure of the printed laminate is still driven by fiber failure; the first-ply failure is attributed to fibers fracturing, and the Onyx delamination occurred during ultimate failure of the laminate.

4.2. Flexural testing

The results from three-point bend testing are given in Table 4. On average, the hand-layup specimens had an ultimate flexural strength of 178.70 MPa, with a standard deviation of 21.8 MPa. The printed parts exhibited an average ultimate flexural strength of 89.46 MPa, with a standard deviation of 9.0 MPa. As in the tension samples, a piecewise linear fit was conducted in the first and second linear sections, to obtain two distinct elastic moduli corresponding to before and after first-ply failure, respectively. In flexure, the laminate failure strain was defined to be the strain at the end of the second linear section, before the unrecoverable drop in load. Fig. 2c–d shows representative flexural stress-strain curves from the hand layup and printed cohorts, respectively.

First-ply failure was also observed in flexure, characterized by a sudden drop-off in load borne by the sample. In all cases, the first-ply failure was followed by a second linear “recovery” period before ultimate laminate failure, which is characterized by a second sudden drop-off, this time without load recovery. In flexure, specimens exhibited a high degree of compliance before failure; this is due to the increase in nose radius on the testing apparatus compared to the ASTM-standard geometry. In general, the Markforged samples exhibited a higher strain-to-failure, with one of the printed specimens not demonstrating ultimate failure within a strain of 6%. By contrast, all the hand-layup samples failed within a strain of 4%. Within both cohorts, the specimens showed varying behavior relating to ultimate flexural stress; in some cases, the sample

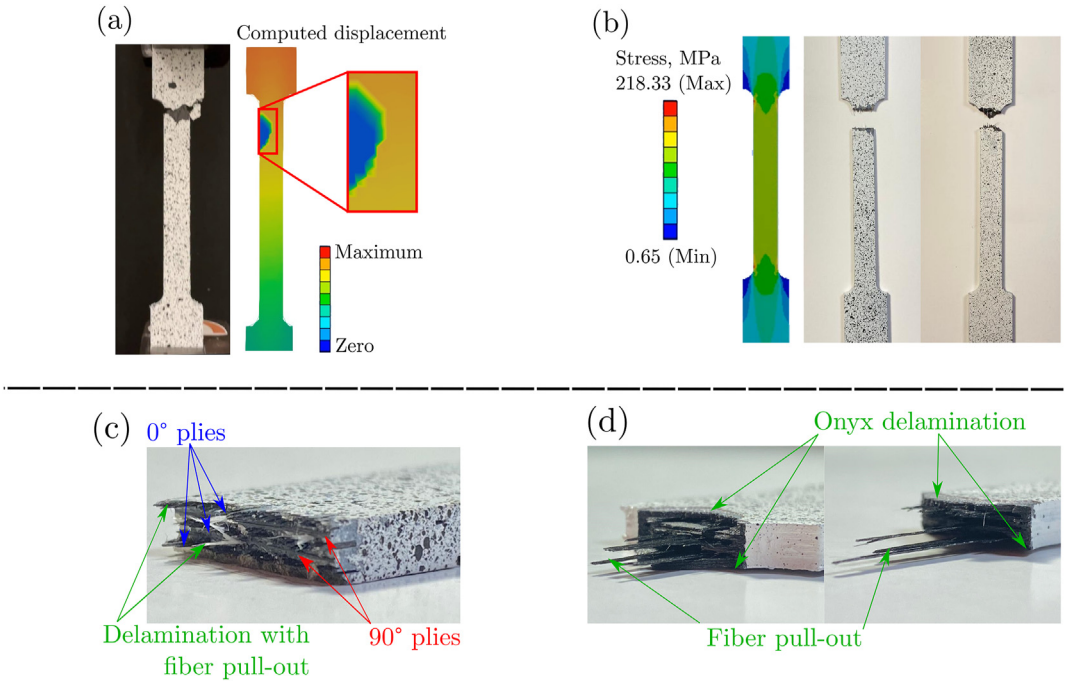

Fig. 3. Analysis of tensile test specimens using (a) digital image correlation to measure displacement and (b) simulation to predict stresses. The simulation showed areas of stress concentration near the neck of the sample, corresponding with the observed site of failure. (c) Failure in a hand-layup sample. (d) Failure in a printed sample.

Table 4
Empirically-determined material properties - flexural testing.

Average values, no V_f normalization	Hand layup, n = 3			Printed, n = 4		
	Mean	St. Dev.	CV	Mean	St. Dev.	CV
Ultimate flexural strength [MPa]	178.70	21.74	0.121	89.46	9.00	0.100
Flexural modulus [MPa]	17898.54	2784.56	0.155	5012.15	238.07	0.047
Flexural modulus after first-ply failure [MPa]	5973.49	907.16	0.151	1533.05	96.08	0.062
First-ply failure strain	0.00498	0.00056	0.112	0.01731	0.00083	0.048
Laminate failure strain	0.02255	0.00493	0.218	0.02717	0.00251	0.092

reached its ultimate flexural stress at the end of the linear-elastic region, whereas other samples were able to support a higher load after the initial yielding strain corresponding to first ply failure.

As observed from the fractured samples, the failure mode of the laminates in flexure was also principally delamination with some degree of fiber pull-out (Fig. 4a). Failure occurred across the width of the laminate, although the failure plane of the samples was not orthogonal to the midplane of the laminate. The failure pattern indicates that some degree of delamination occurred, and it is possible to identify each ply as distinct from the last.

In the printed samples, complete laminate failure did not occur for all samples, primarily due to increased compliance. Some delamination and a high degree of plastic deformation are evident in the laminates that did not fracture (Fig. 4b–c). The top two plies have deformed first as a result of experiencing the strongest compressive stress. This agrees with the data presented in the stress-strain plots; the curves clearly display two drop-off points, but also reflect that the laminate continued to sustain load through the end of the testing period.

The strain-controlled flexure test was also numerically simulated to investigate the deformation and failure behavior of the tested samples (Fig. 4d). In the simulation, the sample was centered on two cylindrical supports of radius 0.5 in. with a corresponding span to thickness ratio of 32:1 determined from the nominal thickness for the hand-layup and printed samples. A third cylindrical object with a nose radius of 0.5 in. and a displacement rate of 2 mm/min was used to apply a bending moment at the center of the sample for 15 min. After 15 min, the cylindrical object was stopped and the sample was allowed to return to an equilibrium position.

In the hand-layup configuration, areas of stress concentration were found at locations symmetric about the centerline of the part when viewed top-down; in the printed samples the stress concentration, and correspondingly the greatest amount of plastic deformation, was localized to the center of the specimen. This could be due to the presence of pure Onyx layers surrounding the layers of cross-ply continuous fiber reinforcement. The simulation results showed good agreement with plastic deformation evident in the physical samples after the flexure test was concluded, indicating that the relative areas of stress and strain concentration throughout the part can be predicted from the models.

4.3. Summary and comparisons

Fig. 5a–b shows the average drop-off in elasticity for each cohort after first ply failure, prior to normalization, with error bars equal to one standard deviation. Normalized material properties as determined by mechanical testing are summarized in Table 5 and Fig. 5c–f. The values were normalized from their raw magnitudes to a fiber volume fraction of 35%. After normalization, it can be seen

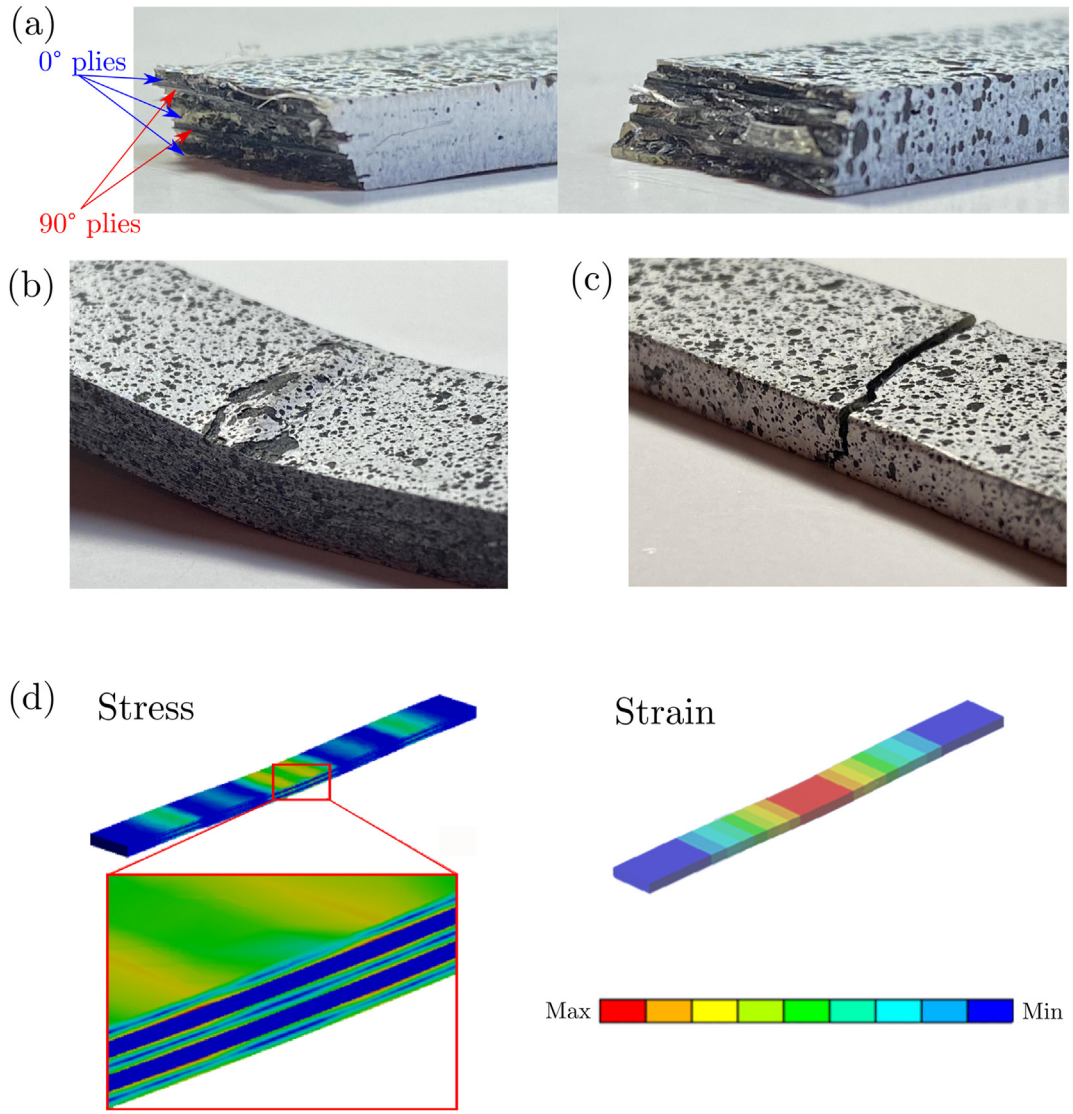

Fig. 4. Analysis of flexural test specimens. (a) Failed hand-layup sample exhibiting delamination and fiber pullout. (b) Some printed samples experienced plastic deformation but did not ultimately fail, whereas the hand-layup samples (c) experienced cracking through the specimen thickness. (d) Simulation of the hand-layup flexure samples, which demonstrated stress concentrations near the center of the sample and at contact points between layers.

that in tension, the printed specimens had (on average) a higher ultimate tensile strength and higher stiffness. However, the hand layup parts demonstrated a higher flexural modulus and higher flexural strength than the printed parts.

The variance among material properties within each sample cohort was also analyzed. Overall, in both the tensile and flexural tests, the Markforged specimens showed greater consistency in behavior during testing compared to the hand-layup samples, indicated by a lower coefficient of variation for each measurement. This was especially true in the flexural samples, with the Markforged samples exhibiting a coefficient of variation of 10% or less across all measured values (Table 4). These findings support the claim that F3DP, like all FFF printing processes, exhibit a high degree of repeatability enforced by automation.

With respect to empirically-determined values, the samples characterized in this study exhibit low stiffness in both tension and flexure compared to specimens tested in the literature [44,45]. The factors that result in this difference are twofold. Primarily, the low fiber volume fraction present in the printed samples results in decreased stiffness and ultimate stress values during testing. It is predicted by the rule of mixtures that increasing the fiber volume fraction linearly increases the stiffness of the material in the longitudinal direction. Additionally, compared to unidirectional laminates, the $[0,90,0,90,0]_T$ orientation of the samples tested in this study necessarily results in a laminate comparatively weaker in the longitudinal direction due to the presence of transversely-oriented plies. Future work may study other symmetric ply configurations, such as an angle-ply $[(+45)_n,(-45)_n]_s$ sequence which is expected to exhibit different failure characteristics.

When compared to the theoretical material properties (section 2.1), material properties obtained from testing were found to be significantly lower (Fig. 5g–h). The difference can be primarily attributed to imperfect bonding between layers, and the presence of void spaces. The theory of laminated beams necessarily assumes perfect bonding between successive plies; thus, the theoretically-predicted results act as an upper bound of physically achievable mechanical properties. In the hand layup process, non-uniform distribution of epoxy resin through the fiber layers creates voided

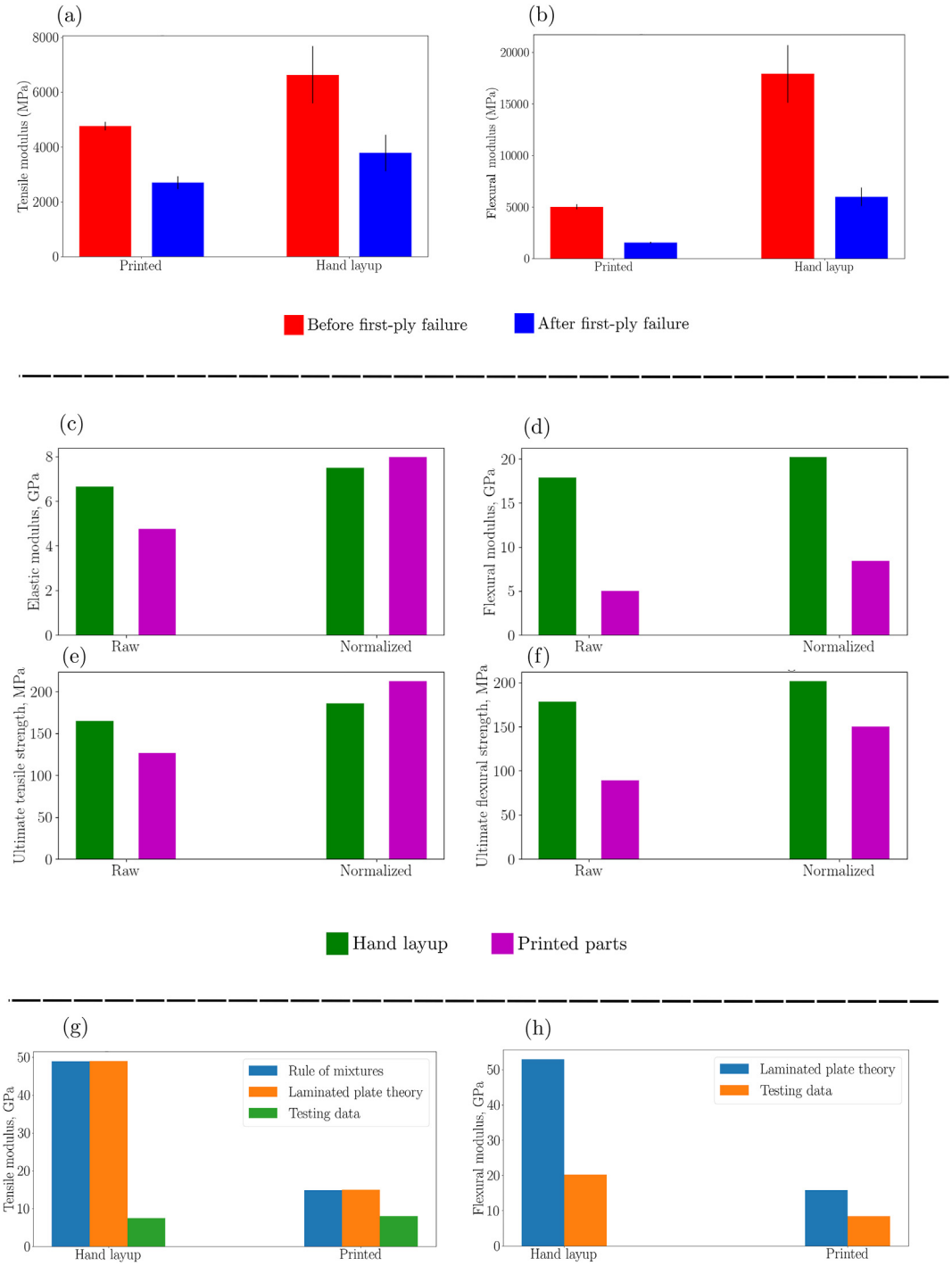

Fig. 5. (a–b): Pre-normalization comparison of average tensile and flexural moduli, respectively, before and after first-ply failure. Error bars indicate one standard deviation. (c–f): Material properties before and after normalization to a fiber volume fraction $V_f = 0.35$. (g–h): Comparison between theoretically-calculated and empirically obtained stiffness values in tension and flexure, respectively.

areas which are relatively weak compared to neighboring locations, in turn acting as "nucleation sites" for ultimate failure. In the printed specimens, void spaces can be attributed to gaps between deposited layers, the degree of which can be controlled by varying print-process parameters including extrusion speed and temperature. In the FFF printing process, voids also form within each layer, originating from the interstitial gaps between successively deposited rows of material. To reduce the space within and between printed layers, "traditional" post-processing techniques such as autoclave post-curing may be considered to finish parts and press out existing voids during the curing process. Despite the presence of voids, stronger bonding within the fiber layers is chemically achieved due to the presence of filler material in the composition of the Markforged proprietary continuous fiber material. Thus, the printed parts were able to more closely approach the values predicted by the laminated beam model than the hand-layup parts.

Table 5
Comparison of composite material properties with normalization.

	Hand layup $V_f = 0.35$	Printed parts $V_f = 0.209$
Elastic modulus, GPa		
Raw	6.628	4.757
Normalized	7.483	7.966
Ultimate tensile strength, MPa		
Raw	164.57	126.88
Normalized	185.805	212.478
Flexural modulus, GPa		
Raw	17.898	5.012
Normalized	20.207	8.393
Ultimate flexural strength, MPa		
Raw	178.7	89.46
Normalized	201.758	149.813

5. Conclusions

In this study, the material properties of cross-ply $[0,90,0,90,0]_T$ laminates manufactured using two methods were compared. In particular, this work aimed to directly compare the wet layup process and the FFF printing of a continuous fiber-reinforced part made entirely using filament extrusion. Laminates were fabricated using both methods and tested in tension and flexure, using the corresponding ASTM standards as a guideline. Much of the existing literature has focused on computing and comparing the material properties of fibers oriented unidirectionally, particularly using unidirectional specimens loaded either parallel or perpendicular to the principal fiber orientation. However, many applications of composite materials benefit from the presence of a cross-ply structure due to the presence of combined, multiaxial loading states.

In reality, part-to-part variability in the production of composites, particularly with respect to the presence of void spaces and imperfect interlaminar bonding, hinders the ability of mathematical and physical models to predict material properties with accuracy; fabrication and testing provide the most accurate point of comparison possible. Testing revealed that for specimens of comparable geometry and fiber stacking sequence, hand-layup samples made with unidirectional carbon fiber and epoxy resin exhibited on average higher ultimate tensile and flexure strengths and stiffnesses than 3D-printed samples made with continuous carbon fiber and a nylon matrix. In general, the hand-layup samples showed greater variability among specimens; however, failure strains were found to be similar between the two cohorts. When these raw values were normalized for fiber volume fraction, the printed composite samples on average were stiffer and had a higher ultimate strength in tension, but the hand-layup samples were still stronger and stiffer in flexure. Future investigation of the void characteristics of hand-layup and printed laminate composites will help to shape more accurate models that can better predict material properties from a theoretical perspective.

Comparing the material properties of these laminates is only one part of the multifaceted design problem of choosing a fabrication method. Engineers must also consider the cost of tooling, fabrication time, and variability among produced parts in order to make the best decision for the application at hand. While existing fabrication methods benefit from manufacturing at scale, decades of experience, and a vast material selection, the advent of fiber 3D-printing shows incredible promise. The F3DP process allows for a high degree of automation, ensures consistency across parts, and provides convenient desktop-manufacturability for rapid prototyping.

Conflicts of interest

The authors declare that there is no conflicts of interest.

Acknowledgements

The authors would like to thank Alex Jordan, Scott McCormick, Katherine Hom, and the staff of the UC Berkeley Mechanical Engineering Machine Shop for their help in facilitating the Markforged printing process and the mechanical testing of specimens. Additionally, the authors acknowledge support from General Motors for funding this research.

References

[1] J. Bauer, S. Hengsbach, I. Tesari, R. Schwaiger, O. Kraft, High-strength cellular ceramic composites with 3d microarchitecture, Proc. Natl. Acad. Sci. Unit. States Am. 111 (2014) 2453–2458, https://doi.org/10.1073/pnas.1315147111.
[2] C. Yang, Y. Kim, S. Ryu, G.X. Gu, Prediction of composite microstructure stress strain curves using convolutional neural networks, Mater. Des. 189 (2020) 9, https://doi.org/10.1016/j.matdes.2020.108509.
[3] G.X. Gu, M. Takaffoli, M.J. Buehler, Hierarchically enhanced impact resistance of bioinspired composites, Adv. Mater. 29 (2017), https://doi.org/10.1002/adma.201700060.
[4] J.W.C. Dunlop, P. Fratzl, Biological composites, Annu. Rev. Mater. Res. 40 (2010) 1–24, https://doi.org/10.1146/annurev-matsci-070909-104421.
[5] C. Chen, G.X. Gu, Generative deep neural networks for inverse materials design using backpropagation and active learning, Adv. Sci. 7 (2020), https://doi.org/10.1002/advs.201902607.
[6] F.C. Campbell Jr., Manufacturing Processes for Advanced Composites, Elsevier, 2003.
[7] P.K. Mallick, Fiber-reinforced Composites: Materials, Manufacturing, and Design, CRC Press, 2007.
[8] B.G. Compton, J.A. Lewis, 3d-printing of lightweight cellular composites, Adv. Mater. 26 (2014) 5930–5935, https://doi.org/10.1002/adma.201401804.
[9] Z. Zhang, K.G. Demir, G.X. Gu, Developments in 4d-printing: a review on current smart materials, technologies, and applications, Int. J. Soc. Netw. Min. 10 (2019) 205–224, https://doi.org/10.1080/19475411.2019.1591541.
[10] J. Frketic, T. Dickens, S. Ramakrishnan, Automated manufacturing and processing of fiber-reinforced polymer (frp) composites: an additive review of contemporary and modern techniques for advanced materials manufacturing, Addit. Manuf. 14 (2017) 69–86.
[11] F. Libonati, G.X. Gu, Z. Qin, L. Vergani, M.J. Buehler, Bone-inspired materials by design: toughness amplification observed using 3d printing and testing, Adv. Eng. Mater. 18 (2016) 1354–1363, https://doi.org/10.1002/adem.201600143.
[12] X. Tian, T. Liu, C. Yang, Q. Wang, D. Li, Interface and performance of 3d printed continuous carbon fiber reinforced pla composites, Compos. Appl. Sci. Manuf. 88 (2016) 198–205, https://doi.org/10.1016/j.compositesa.2016.05.032.
[13] W. Zhong, F. Li, Z. Zhang, L. Song, Z. Li, Short fiber reinforced composites for fused deposition modeling, Mater. Sci. Eng., A 301 (2001) 125–130, https://doi.org/10.1016/s0921-5093(00)01810-4.
[14] X. Zhang, W. Fan, T. Liu, Fused deposition modeling 3d printing of polyamide-based composites and its applications, Compos. Commun. 21 (2020) 3, https://doi.org/10.1016/j.coco.2020.100413.
[15] R. Matsuzaki, M. Ueda, M. Namiki, T.-K. Jeong, H. Asahara, K. Horiguchi, T. Nakamura, A. Todoroki, Y. Hirano, Three-dimensional printing of continuous-fiber composites by in-nozzle impregnation, Sci. Rep. 6 (2016), https://doi.org/10.1038/srep23058.
[16] Y. Nakagawa, K. Mori, T. Maeno, 3d printing of carbon fibre-reinforced plastic parts, Int. J. Adv. Manuf. Technol. 91 (2017) 2811–2817, https://doi.org/10.1007/s00170-016-9891-7.
[17] F. Ning, W. Cong, J. Qiu, J. Wei, S. Wang, Additive manufacturing of carbon fiber reinforced thermoplastic composites using fused deposition modeling, Compos. B Eng. 80 (2015) 369–378, https://doi.org/10.1016/j.compositesb.2015.06.013.
[18] Z. Liu, Q. Lei, S. Xing, Mechanical characteristics of wood, ceramic, metal and carbon fiber-based pla composites fabricated by fdm, J. Mater. Res. Technol. 8 (2019) 3741–3751, https://doi.org/10.1016/j.jmrt.2019.06.034.
[19] E. Yasa, K. Ersoy, Dimensional accuracy and mechanical properties of chopped carbon reinforced polymers produced by material extrusion additive manufacturing, Materials 12 (2019) 3885, https://doi.org/10.3390/ma12233885.
[20] J. Naranjo-Lozada, H. Ahuett-Garza, P. Orta- Castañón, W.M.H. Verbeeten, D. Sáiz-González, Tensile properties and failure behavior of chopped and continuous carbon fiber composites produced by additive manufacturing, Additive Manuf. 26 (2019) 227–241, https://doi.org/10.1016/j.addma.2018.12.020.
[21] https://markforged.com/3d-printers/x7. Accessed December 2020.

[22] L.G. Blok, M.L. Longana, H. Yu, B.K.S. Woods, An investigation into 3d printing of fibre reinforced thermoplastic composites, Additive Manuf. 22 (2018) 176–186, https://doi.org/10.1016/j.addma.2018.04.039.
[23] M. Spoerk, C. Savandaiah, F. Arbeiter, G. Traxler, L. Cardon, C. Holzer, J. Sapkota, Anisotropic properties of oriented short carbon fibre filled polypropylene parts fabricated by extrusion-based additive manufacturing, Compos. Appl. Sci. Manuf. 113 (2018) 95–104, https://doi.org/10.1016/j.compositesa.2018.06.018.
[24] H.L. Tekinalp, V. Kunc, G.M. Velez-Garcia, C.E. Duty, L.J. Love, A.K. Naskar, C.A. Blue, S. Ozcan, Highly oriented carbon fiber–polymer composites via additive manufacturing, Compos. Sci. Technol. 105 (2014) 144–150, https://doi.org/10.1016/j.compscitech.2014.10.009.
[25] J.M. Chacón, M.A. Caminero, P.J. Núñez, E. García-Plaza, I. García-Moreno, J.M. Reverte, Additive manufacturing of continuous fibre reinforced thermoplastic composites using fused deposition modelling: effect of process parameters on mechanical properties, Compos. Sci. Technol. 181 (2019), https://doi.org/10.1016/j.compscitech.2019.107688.
[26] A.N. Dickson, J.N. Barry, K.A. McDonnell, D.P. Dowling, Fabrication of continuous carbon, glass and kevlar fibre reinforced polymer composites using additive manufacturing, Additive Manuf. 16 (2017) 146–152, https://doi.org/10.1016/j.addma.2017.06.004.
[27] C. Badini, E. Padovano, R. De Camillis, V.G. Lambertini, M. Pietroluongo, Preferred orientation of chopped fibers in polymer-based composites processed by selective laser sintering and fused deposition modeling: effects on mechanical properties, J. Appl. Polym. Sci. 137 (2020), https://doi.org/10.1002/app.49152.
[28] M. Elkington, D. Bloom, C. Ward, A. Chatzimichali, K. Potter, Hand layup: understanding the manual process, Adv. Manuf. Polym. Compos. Sci. 1 (2015) 138–151, https://doi.org/10.1080/20550340.2015.1114801. URL:.
[29] S.V. Hoa, Principles of the Manufacturing of Composite Materials, DEStech Publications, Inc, 2018.
[30] M. Somireddy, C.V. Singh, A. Czekanski, Analysis of the material behavior of 3d printed laminates via FFF, Exp. Mech. 59 (2019) 871–881, https://doi.org/10.1007/s11340-019-00511-5.
[31] R.F. Gibson, Principles of Composite Material Mechanics, fourth ed., CRC Press, 2016.
[32] A.T. Nettles, Basic Mechanics of Laminated Composite Plates, NASA, Marshall Space Flight Center, 1994.
[33] R.M. Guedes, J. Xavier, Understanding and predicting stiffness in advanced fibre-reinforced polymer (FRP) composites for structural applications, in: Advanced Fibre-Reinforced Polymer (FRP) Composites for Structural Applications, 2013, pp. 298–360, https://doi.org/10.1533/9780857098641.3.298.
[34] S.W. Tsai, Mechanics of Composite Materials: Part 1 - Introduction, Air Force Materials Laboratory, Research and Technology Division, Air Force Systems Command, 1966.
[35] R. Jones, Mechanics of Composite Materials, CRC Press, 1998.
[36] N.J. Pagano, Analysis of the flexure test of bidirectional composites, J. Compos. Mater. 1 (1967) 336–342, https://doi.org/10.1177/002199836700100402.
[37] F. Ghebretinsae, O. Mikkelsen, A.D. Akessa, Strength analysis of 3d printed carbon fibre reinforced thermoplastic using experimental and numerical methods, IOP Conf. Ser. Mater. Sci. Eng. 700 (2019), 012024, https://doi.org/10.1088/1757-899x/700/1/012024.
[38] Material Datasheet: Composites. Revision 3.1, Markforged, Watertown, MA, 2019.
[39] F. van der Klift, Y. Koga, A. Todoroki, M. Ueda, Y. Hirano, R. Matsuzaki, 3d printing of continuous carbon fibre reinforced thermo-plastic (cfrtp) tensile test specimens, Open J. Compos. Mater. 6 (2016) 18–27, https://doi.org/10.4236/ojcm.2016.61003.
[40] P. Damodaram, R. Mitra, Bio-mimetic Design with 3d Printable Composites, Electronic Theses and Dissertations 2443, 2018. URL: https://openprairie.sdstate.edu/etd/2443.
[41] ASTM D3039/D3039M-17, Standard Test Method for Tensile Properties of Polymer Matrix Composite Materials, ASTM International, West Conshohocken, PA, 2017. www.astm.org.
[42] ASTM D7264/D7264M-15, Standard Test Method for Flexural Properties of Polymer Matrix Composite Materials, ASTM International, West Conshohocken, PA, 2015. www.astm.org.
[43] D. Turner, Digital Image Correlation Engine (DICe) Reference Manual, Sandia Report, SAND2015-10606 O, 2015.
[44] T.A. Dutra, R.T.L. Ferreira, H.B. Resende, A. Guimarães, Mechanical characterization and asymptotic homogenization of 3d-printed continuous carbon fiber-reinforced thermoplastic, J. Braz. Soc. Mech. Sci. Eng. 41 (2019), https://doi.org/10.1007/s40430-019-1630-1.
[45] G.D. Goh, V. Dikshit, A.P. Nagalingam, G.L. Goh, S. Agarwala, S.L. Sing, J. Wei, W.Y. Yeong, Characterization of mechanical properties and fracture mode of additively manufactured carbon fiber and glass fiber reinforced thermoplastics, Mater. Des. 137 (2018) 79–89, https://doi.org/10.1016/j.matdes.2017.10.021.